CrossMark

ORIGINAL PAPER

The Effect of Lineation on Anisotropy in Dry and Saturated Himalayan Schistose Rock Under Brazilian Test Conditions

Jagadish Kundu[1] · Bankim Mahanta[2,3] · Kripamoy Sarkar[1] · T. N. Singh[2]

Abstract The paper presents experimental observations of the anisotropic effect of dry and saturated lineated schistose rock on deformational behaviour and fracture patterns under indirect tensile loading conditions. Dry mylonitic quartz–mica schist (M-QMS) shows strength minima in between lineation orientation of 20°–30° with loading direction, whereas dry crenulated quartz–mica schist (C-QMS) shows strength minima in between 45° and 60°. Water saturation significantly reduces the failure strength and shifts the strength minima towards a higher angle. In addition, the water saturation effect induces plasticity along the lineation direction. P-wave velocity is found to be maximum along lineation direction, which continuously decreases to a minimum value across the lineation. Three types of fracture patterns, namely layer activation, central and non-central, are observed for both the rock types. For both the rock types, tensional fractures occur when the lineation is inclined at 0° and 90° to the loading direction, whereas shear and mixed-mode fractures occur at all other orientations. Fracture through the layer activation is prominent in saturated specimens compared to the dry specimens for β angle range of 15°–60° and 15°–45° in the case of M-QMS and C-QMS, respectively.

1 Introduction

The hilly terrains of Himachal Pradesh in India are considered to have major potential for hydroelectricity due to the presence of five perennial river basins and sufficient headwater in the state. Till date, nine projects have been completed and are successfully harnessing electricity from the Himalayan Rivers. Many underground excavations have been planned and are under construction in the hills of Himachal Pradesh in order to exploit hydroelectricity. Formations in the area contain varied lithology and anisotropic rocks, which are always troublesome to geotechnical engineers in underground as well as open excavations such as cut slopes (Kundu et al. 2016a; Mahanta et al. 2016a). Most metamorphic rocks and laminated sedimentary rocks are considered to be anisotropic and heterogeneous (Gholami and Rasouli 2014; Hoek 1964; Khanlari et al. 2015; Mahanta et al. 2016b; McLamore and Gray 1967; Nasseri et al. 2003; Singh et al. 2015; Tavallali 2010; Tavallali and Vervoort 2013). Though stress distribution in isotropic rock is well understood, a poor understanding of anisotropic rocks affects the performance of the tunnel boring machine (TBM) as well as excavation of cavern using drill blast method (Gong et al. 2005). Boreholes, in the case of petroleum, mining and geothermal applications, are also rigorously affected by the anisotropic effect of rocks (Stjern et al. 2003). In situ stress development and the deformational behaviour of rock and materials are the most important considerations for any design and constructions in a rock mass. However, the understanding of these aspects in isotropic rock masses has developed to a

✉ Bankim Mahanta
  bankim42mahanta@gmail.com

[1] Department of Applied Geology, Indian Institute of Technology (Indian School of Mines) Dhanbad, Dhanbad, Jharkhand, India

[2] Department of Earth Sciences, Indian Institute of Technology Bombay, Mumbai, Maharashtra, India

[3] IITB-Monash Research Academy, Indian Institute of Technology Bombay, Mumbai, Maharashtra, India

considerable level, which enables the solving of most of the problems in the civil, mining and petroleum sectors. Despite long research history, anisotropic rocks have always commanded the attention of the geotechnical fraternity for the complexity and criticality of the behaviour of the rocks. The directional behaviour of anisotropic rock material towards various physical, mechanical, hydraulic, thermal and dynamic properties needs to be understood for better designing of underground excavation projects, cut slopes and bore holes and, especially, their numerical modelling (Tavallali and Vervoort 2010a).

Reviews of work on rock anisotropy trace back to the 1940s when Casagrande and Carillo (1944) first modelled strength anisotropy in the soil, followed by Jaeger (1960), who presented the continuously variable shear strength theory for transversely isotropic rocks. Jaeger (1960) also suggested that there is only one possible plane of failure at which the shear strength is minimum. Experimental evidences by Donath and Cohen (1960) also suggest possible failure on a single plane, but with negligible effect of anisotropy when the inclination of the isotropic layers with the principal stress direction is more than 30°. Further experiments of Donath (1961) on a planar anisotropic rock under low confining pressure show that the effect is significant up to a transversely isotropic layer inclination of 60° with the loading direction. He also suggested a concave upward (parabolic) curve for the failure strength versus inclination angle, with the minimum strength occurring around 30°. Salamon (1968) described five elastic moduli (which are sufficient to define a transversely isotropic material) in terms of thickness and properties of strata in the rock mass. Similar works have been performed by Wardle and Gerrard (1972) in order to produce charts for quick assessment of elastic properties of transversely isotropic rock masses that are limited to a range of two material systems. Tests on the shear strength of saprolite schist by Ogunsanwo (1986) show the highest strength across the schistosity and the lowest strength along the schistosity. Amadei et al. (1987) and Pan et al. (1994, 1995) have addressed the effect of transverse anisotropy on magnitude and distribution of gravitational stress. Amadei (1996) has discussed the deformability of anisotropic rocks and the stress distribution in them. The effect of the orientation of a single joint on the loading direction in the specimen made up of plaster of Paris and sandstone shows that increasing the confinement diminishes the effect of the joint and occurrence of the minimum strength at a lower confinement at an inclination of approximately 30° (Ramamurthy and Arora 1994). Talesnick et al. (1995) attempted an analytical framework in combination with laboratory testing of a single hollow cylindrical rock specimen in order to determine elastic parameters of transversely isotropic rock. Zhang et al. (2011) have conducted systematic laboratory tests on Danba quartz–mica schist to study the anisotropic effect in tensile strength, uniaxial compressive strength; unloading and long-term stress states. The P-wave velocity in the direction parallel to the schistose planes was found three times higher compared to the direction normal to the schistose plane. Additionally, they have also reported that under uniaxial compression, cracks develop quite easily when loaded parallel to the schistose direction than any other loading direction. Fereidooni et al. (2015) have experimented the effect of confining pressure on transverse anisotropy of rock and found that the anisotropy angle corresponding to minimum strength shifts to a higher value with higher confining pressure. Kim et al. (2016) have found that with increasing angle of bedding planes of transversely isotropic cross-bedded Berea sandstones, there is a continuous decrease in strength. However, simulation through 2D particle flow code (PFC-2D) shows highest crack numbers (in the case of both tensile and shear fracture) in the loose layers when beddings are inclined at an angle of 30° from horizontal. Zhang et al. (2015) have reported a strong anisotropy with minimum strength index (point load strength index) when loaded parallel to the schistosity plane and maximum strength index when loaded perpendicular to the schistosity plane. Furthermore, the fracture planes are zigzag when a failure occurs across the plane and flat and smooth when failed along the weaker plane. Lin et al. (2016) have performed a series of hydraulic fracture experiments on shale to examine the anisotropic effect on the propagation of fractures. It is reported that the breakdown pressure is highest at a bedding plane angle of 0° and lowest at a bedding plane angle of 90°.

Hydrocarbon recovery and geothermal energy exploitations are achieved through hydraulic fracturing, which creates tensile fractures in the host rock (Mighani et al. 2016). Therefore, it is necessary to understand the tensile behaviour of rocks for appropriate planning and design. Many researchers have pointed out the effect of transversely isotropic rock on tensile strength of the rock by diametrical compression. McLamore and Gray (1967), Chen et al. (1998), Claesson and Bohloli (2002), Cai and Kaiser (2004), Vervoort et al. (2014) and Tan et al. (2015) have studied the effect of anisotropic layer orientation on the diametrical loading direction of disc-shaped specimens. Similar studies have been carried out by Chen et al. (1998), Tavallali and Vervoort (2010a, b) and Khanlari et al. (2015) on layered sandstone; Barla and Innaurato (1973) on gneiss and schist; Debecker and Vervoort (2009), Tan et al. (2015) and Mighani et al. (2016) on shale; Hobbs (1964) on siltstone; and Gholami and Rasouli (2014) on slate. Though there has been a lot of research on rocks that have an

anisotropic character, experiments on the behaviour of lineated and crenulated rocks are absent in the literature.

In this paper, diametrical loading tests in a Brazilian cage have been carried out on one set of lineated and one set of crenulated schist at different orientations of lineation and crenulation axis in relation to the loading direction. The tests were carried out in both dry and saturated conditions. The effects of anisotropy on Brazilian tensile strength and fracture pattern are studied for both types of rocks. In addition, the strain variations along lineation direction are well observed for different orientations. Different types of fracture patterns have been identified as a function of lineation orientation. The effect of saturation on the strength, the deformational behaviour and the anisotropy trend have been documented further. Variation in P-wave velocity with respect to lineation direction is also measured for both the rock types. One block sample, with mylonitic lineation, and the other with crenulations that had both intersection and crenulation lineation, were collected from Jhakri region of Himachal Pradesh, which is close to hydroelectric power project of Satluj Jal Vidyut Nigam Ltd.

2 Geology of the Study Area

The study area is situated in the Lesser Himalayan region of Himachal Pradesh and consists of rocks from the Jutogh group of formations (Singh 1979). The Jutogh Nappe tectonically overlies the autochthonous Rampur Group and Wangtu Gneissic Complex (Pandey et al. 2004). The Jutogh formation is considered as allochthonous to para-utochthonous and has slid over the Jutogh thrust on to the Rampur series (Bhargava 1972). The Jutogh group of rocks have undergone tectonic detachment through ductile shearing (Mukhopadhaya et al. 1997). Singh (1979) named this ductile shear detachment as the Jeori dislocation. Lithostratigraphy of the Jutogh group of rocks reported by Bhargava (1972) in the normal order of superposition of the rocks is presented in Table 1.

The rock types encountered in the area are mylonites of quartz–mica schist, garnet-bearing quartz–mica schist and muscovite–biotite schist. Other lithotypes include augen migmatite, biotite gneiss and amphibolites (Kundu et al. 2016b; Singh 1979). A geological map illustrating the study area is presented in Fig. 1.

3 Material and Method

In order to observe the directional effects of lineation on the strength and strain of rocks, two rock types have been selected: block-1, mylonitic schist, and block-2, crenulated

Table 1 Stratigraphy of Jutogh formation in its normal order of superposition (Bhargava 1972)

Pink to grey concordant granite (intrusive)	
Schist member	Brown to yellowish-brown garnetiferous biotite schist, gneiss, garnetiferous quartzite
	Dark brown to light brown biotite schist, quartz schist
	quartz–mica schist, sericite schist, chlorite phyllite amphibolite
Gneiss member	Biotite gneiss, grey to buff augen and streaky
	Gneiss. Bands of biotite schist
Carbonaceous member	Dark grey carbonaceous schist at places graphitic, sporadically pyritous
	White to grey quartzite bands and grey limestone bands, amphibolite

schist. The former consists of mylonitised quartz–mica schist with well-preserved L tectonites, and the latter is a crenulated quartz–mica schist. Mylonites that occur in high-strain zones due to a crystal-plastic deformation process, is a good evidence of ductile shearing (Hobbs et al. 1976; Passchier and Trouw 2005). The mylonitic structure in shear zones is predominantly fine grained in comparison with wall rocks and contains a fabric of stretching lineation on the foliations plane (Passchier and Trouw 2005). These rocks contain porphyroclasts, which are of relatively higher stiffness than the groundmass and may indicate shear sense, although not necessarily. However, planner foliations in the collected samples have been obliterated probably due to younger phases of deformations. The foliations, however, show very good stretching lineation and sigmoidal shear sense indicator (SSI). Block-2 is a crenulated quartz–mica schist that shows the zonal crenulation cleavage that is marked by M-domains (cleavage domains), which serve as unbroken fold limbs that bridge the continuous cleavage of adjacent microlithons. The M-domains are the dark and zones of fine-grained micaceous minerals.

Microlithon domains are comparatively lighter-coloured, coarse-grained and have laminae of quartz and micaceous minerals. The evolution of the crenulation cleavage starts with a shortening of the laminae that is parallel to the continuous cleavages in the direction of the maximum compressive force. Shortening due to compression is accommodated by progressive deformation through physical and/or chemical transportation of limb materials, which leads to the crenulation cleavage (Gray and Durney 1979). The deformation process along with ultimate fold forms is governed by the thickness and a mechanical characteristic of continuous cleavage laminae, shear strength parameters between multilayers and magnitude of shortening (Davis et al. 2012). Crenulations are inherited
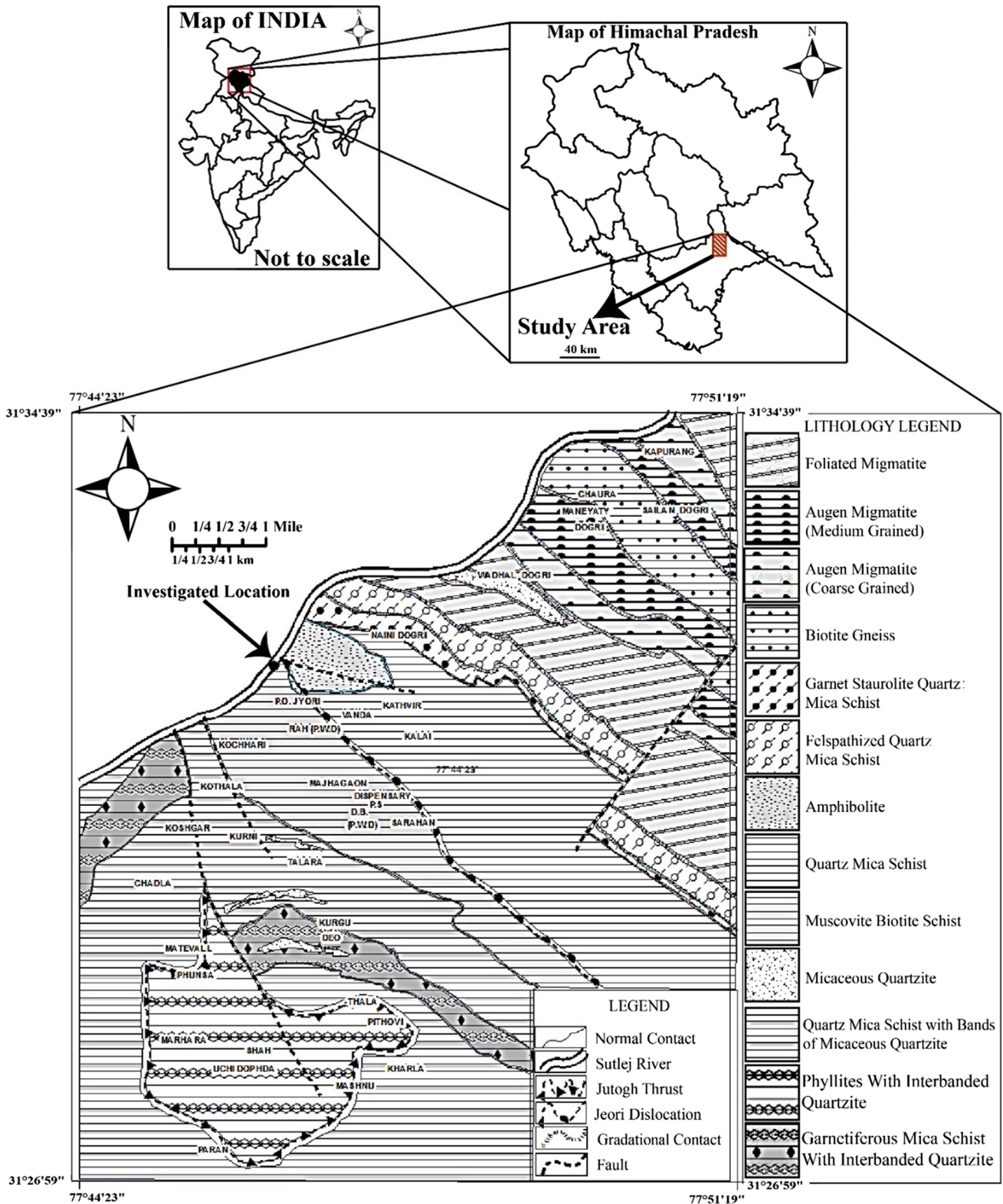
Fig. 1 Geological map of Sarahan Bushair area, Shimla, Himachal Pradesh, India (after Singh 1979)

by two types of lineation such as intersection lineation and crenulation lineation. The former is the intersection line between the continuous cleavage of microlithons and any plane that is parallel to the crenulation axis, whereas the latter is defined by closely spaced crests and troughs of minor folds (fold hinges). Crenulation lineation is an array

Table 2 Physical properties of the samples from block-1 and block-2

Properties	Block-1	Block-2
Water absorption (%)	0.91	0.68
Dry density (g/cm^3)	2.77	2.71
Saturated density (g/cm^3)	2.79	2.73
Porosity (%)	2.52	1.86

of straight to slightly curved, discontinuous crests and troughs of folds (Davis et al. 2012). The physical properties of the samples are described in Table 2. The core samples were extracted from the intact and fracture-free blocks, and the experiments were carried out in disc specimens under Brazilian test conditions. The methodology, followed for the experiment, is presented in Fig. 2.

4 Petrography and X-Ray Diffraction

4.1 Petrography

Optical examination of the thin sections from block-1 indicates the predominant presence of quartz and biotite, with a small amount of muscovite. Plagioclase laths could not be identified through petrographic study, but later on, its presence at a small percentage was confirmed through X-ray diffraction (XRD) analysis (Fig. 3). The fabric shows the signature of dynamic recrystallisation. Large recrystallised quartz grains show a sigmoidal shear sense and are surrounded by a groundmass of quartz and mica. The overall fabric corresponds to the mylonitic structure. Block-2 exhibits the presence of quartz, muscovite and biotite. A few plagioclase feldspars in the form of small laths are also visible. However, most of the plagioclase laths alter to sericite and many are in the alteration process, which make them optically unrecognisable (their presence is confirmed by XRD analysis). Recrystallised quartz grains are separated by mica layers and undergo a crenulation phase. Figure 4 demonstrates the photomicrographs of thin sections prepared from block-1 and block-2.

4.2 XRD

Small chips of the samples were collected separately from each block and were then crushed to fine powders using an agate mortar and pestle. The powders, after passing through a 40-μm sieve, were collected in a glass container and sent for XRD analysis. Diffractograms for the samples
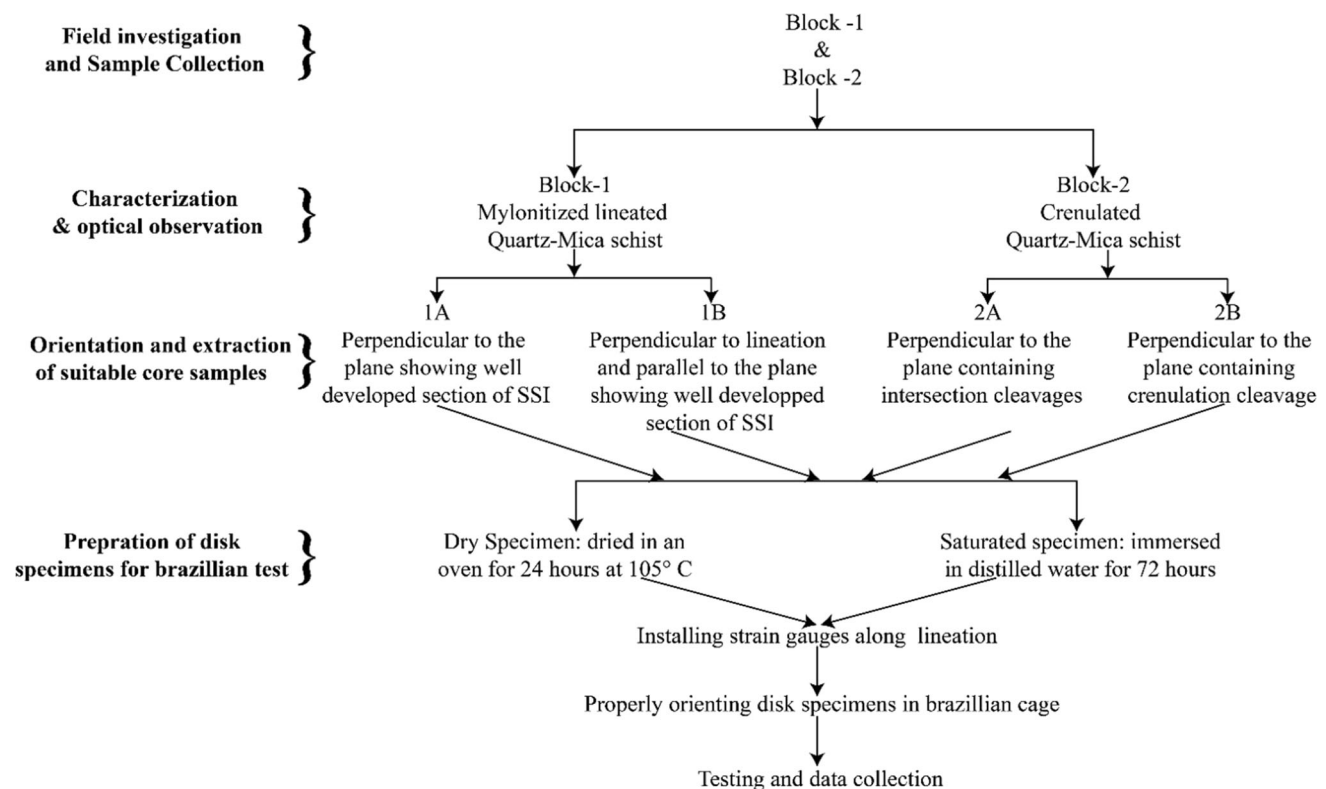

Fig. 2 Schematic diagram describing the complete methodology followed in the experimental work
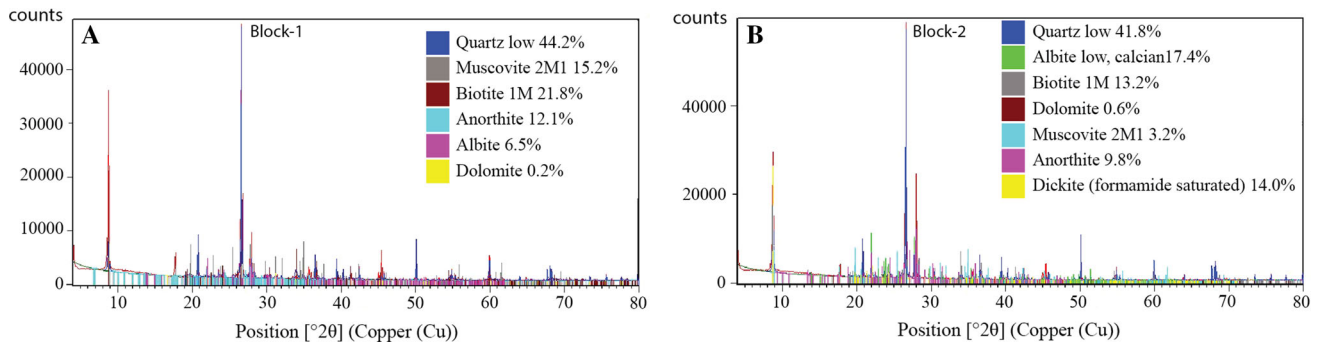
Fig. 3 The X-ray diffractogram for quantitative powder diffraction analysis. **a** Mylonitised quartz–mica schist (*block-1*) shows comparatively higher mica percentage, **b** crenulated quartz–mica schist (*block-2*) showing comparatively lower mica percentage
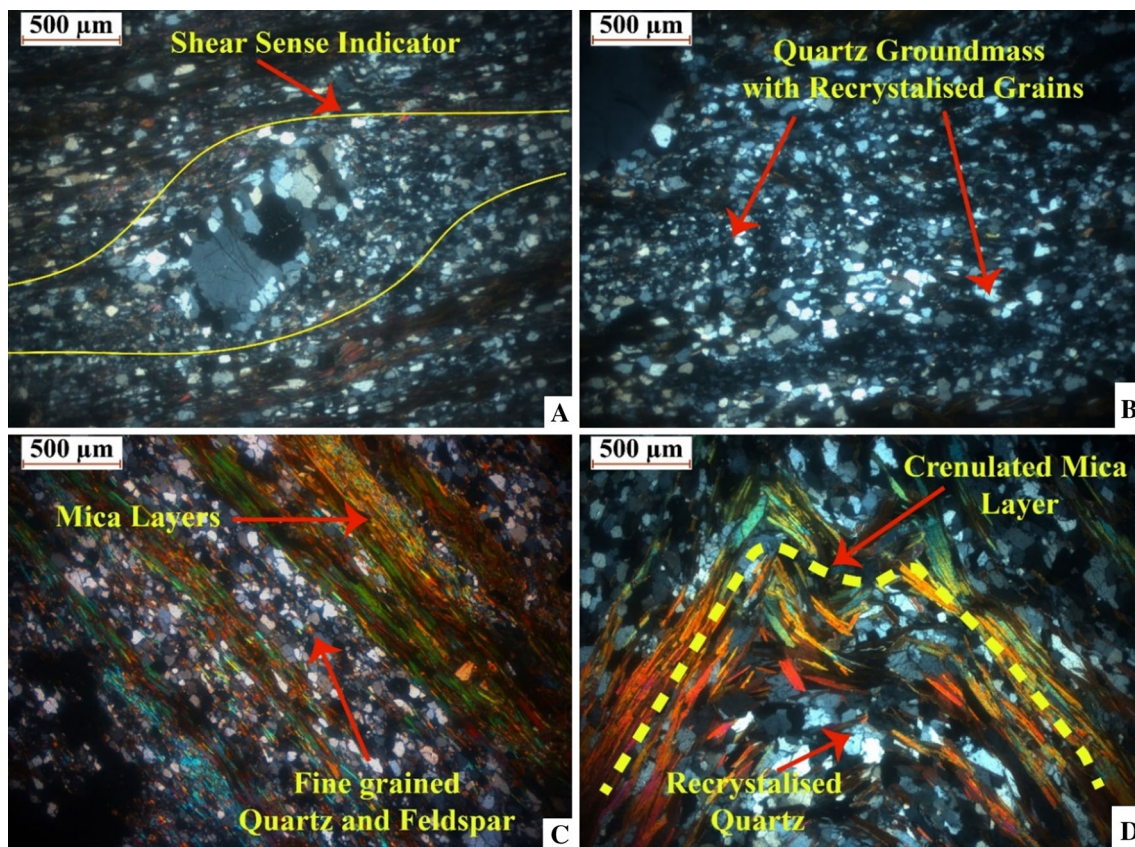

Fig. 4 Photomicrographs of the prepared thin sections of collected samples; **a** rotation of quartz porphyroclast indicating dextral shear sense in M-QMS (*block-1*); **b** recrystallised fine-grained quartz in M-QMS; **c** alternating mica and quartzo-feldspathic layer in C-QMS (*block-2*); **d** crenulated mica layer and recrystallised quartz grain in C-QMS

are given in Fig. 3. The analysis for block-1 shows the presence of 44.2% of quartz, 15.2% of muscovite, 21.8% of biotite, 6.5% of albite, 12.1% of anorthite and 0.2% of dolomite, whereas block-2 consists of 41.8% of quartz, 17.4% of calcian albite, 13.2% of biotite, 3.2% of muscovite, 9.8% of anorthite, 14% of dickite and 0.6% of dolomite.

5 Specimen Preparation and Experimental Set-up

5.1 Specimen Preparation

In order to prepare specimens for the Brazilian test, the blocks were oriented as per the requirement and were then drilled through with a diamond core bit that had an inner
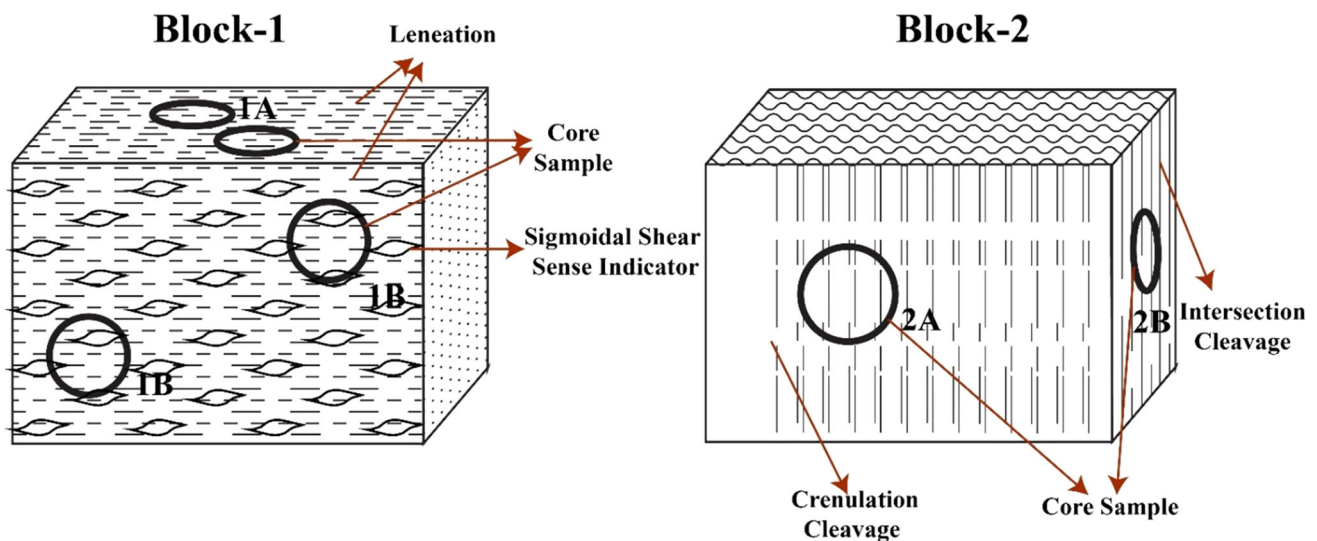
Fig. 5 Schematic diagram of block-1 and block-2, representing the orientation of the core samples (not to scale)

diameter of 50 mm. Sigmoidal SSI was clearly visible parallel to lineation in M-QMS (block-1). As illustrated in Fig. 5 block-1, the rock was drilled in two orthogonal directions that were perpendicular to the lineation. A plane on which the sigmoidal SSI is perfectly developed (1B) and another plane orthogonal to it (1A) were selected. The block was carefully drilled perpendicular to these planes. The block was traversed by some irregular fractures. So proper care was taken during drilling not to include fractures in the core. The cored samples were named as 1B and 1A, respectively. The C-QMS (block-2) was also cored in two orthogonal directions that were perpendicular to the crenulation axis (Fig. 5; block-2). Cores were drilled in two orthogonal planes: one perpendicular to the plane that contained the intersection cleavages (2B) and another perpendicular to the plane that contained the crenulation cleavage (2A) (Fig. 5). The cored samples were named 2B and 2A, respectively. Thus, four subtypes of rock samples were obtained from two types of blocks.

The cored samples were then air-dried and cut into discs of 25 mm thickness according to ASTM standard (ASTM D3967-08, 2008) in order to prepare the specimens for the Brazilian indirect tensile tests. The curved surfaces of the specimens were examined for any imperfections, and inappropriate samples were discarded. A total of 112 specimens (28 specimens from each of 1A, 1B, 2A and 2B) were selected for the test, out of which 56 (14 specimens from each of 1A, 1B, 2A and 2B) were kept in an oven for 24 h at 105 °C and 56 (14 specimens from each of 1A, 1B, 2A and 2B) were submerged in distilled water for saturation. The percentage of unforced water absorption (A_w) in both the rock types was determined by the formula as follows:
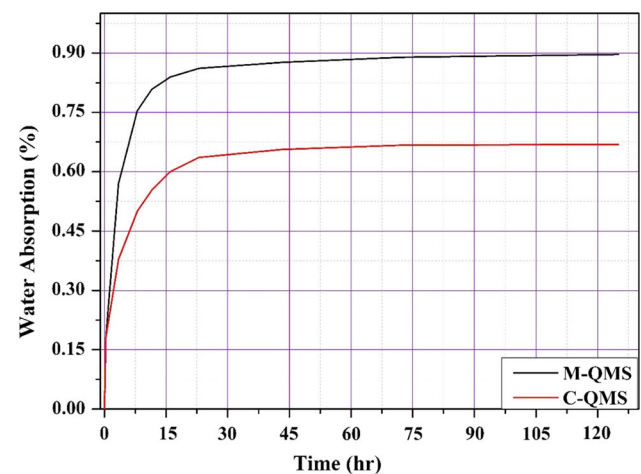

Fig. 6 Water absorption for both the rocks with time

$$A_w = \frac{(M_{wet} - M_{dry})}{M_{dry}} \times 100\%$$

where M_{wet}: mass of wet surface-dried sample in air at a specific time interval, and M_{dry}: mass of oven-dried sample in air at a specific time interval.

The unforced water absorption with time has been graphically represented in Fig. 6. It has been noticed that M-QMS (with 37% mica content) has almost reached equilibrium after 72 h, whereas the C-QMS (with 16.4 mica content) has reached equilibrium after 40 h.

5.2 Experimental Set-up

Apart from the direct tensile test, which is very difficult to carry out in practice, several methods have been
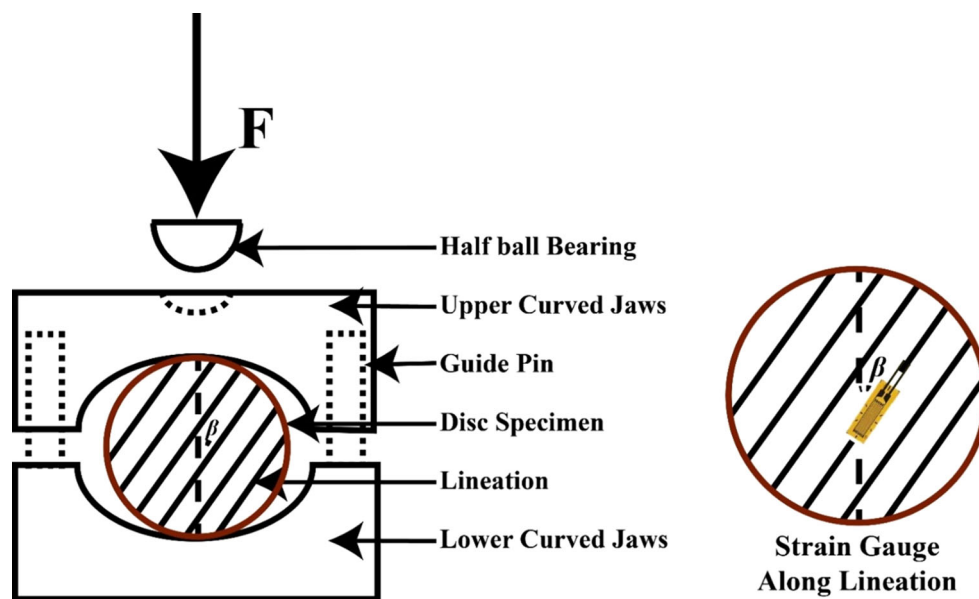
developed for indirect tensile strength testing of rock
materials, such as the bending test, the hoop test, the
indentation test, the diametrical compression test and the
ring test (Chen and Hsu 2001; Hobbs 1964, 1965; Hudson
1969; Nova and Zaninetti 1990). Among all these meth-
ods, the Brazilian tensile strength (BTS) test (diametrical
compression test) is a simple, indirect method for iso-
tropic, homogeneous, linearly elastic and brittle materials
(Mellor and Hawkes 1971) such as coal (Berenbaom and
Brodie 1959), concrete and rocks (Li and Wong 2013). So
far, four typical loading configurations of the Brazilian
test are proposed, which are flat loading platens, flat
loading platens with two small diameter steel rods, flat
loading platens with cushioning and curved loading jaws
(Li and Wong 2013; Mellor and Hawkes 1971). In these
methods, it is assumed that failure occurs at the point of
maximum tensile stress (Fairhurst 1964). The Brazilian
tensile test has been adopted in this study for indirect
determination of the tensile strength. According to ISRM
(1981), the sample was kept in between two opposed
concave steel loading jaws coupled by two guide pins so
that the contact of the arc with the sample surface makes
an angle of 10° at failure (Fig. 7). A half ball bearing
system was arranged on the upper surface of the upper
jaw to execute perfect uniaxial loading. The whole
arrangement was kept between two parallel loading pla-
tens of a Universal Testing Machine (UTM) that had a
capacity of 400 kN, and continuous loading was applied
at a rate of 200 N/s. A load cell with a 50-kN capacity
was installed for precise recording of the load data.

Disc specimens were kept in a specified orientation at
which the inherent lineation makes an angle (β) with the
loading direction, as illustrated in Fig. 7. To observe the

directional behaviour of anisotropy, experiments were
carried out at seven different orientations for each subtype
(that is, 1A, 1B, 2A and 2B) by keeping the specimen at a β
angle of 0°, 15°, 30°, 45°, 60°, 75° and 90°. Out of 14 dry/
wet specimens of each subtype, electrical resistance strain
gauges were installed in seven specimens (one for each
orientation) to monitor the strain along the lineation of the
samples during loading, as illustrated in Fig. 7 (right). The
load cell and the strain gauge were connected to a suit-
able data logger for continuous recording of load and
microstrain. The samples were immersed in distilled water
for 72 h in order to determine the effect of water saturation
on rock strength (Fig. 8), failure strain (Fig. 9) and P-wave
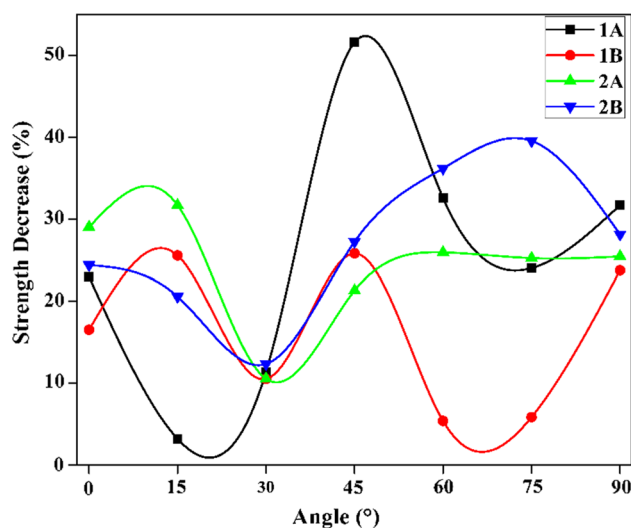velocity (Fig. 10).

Fig. 8 Graph representing peak strength reduction percentage as a
result of saturation at all orientations for specimen subtypes

In order to observe anisotropy in P-wave velocity, the block samples were cut into rectangular cuboids of 15 cm length, 15 cm width and 6 cm height. The longitudinal edge of each cuboid was cut at specified β angles. So four specimens were prepared to measure P-wave velocity at a β angle of 0°, 15°, 30°, 45°, 60°, 75° and 90°. The velocity was measured using UPV (ultrasonic pulse velocity) test instrument, Pundit Lab (Proceq) with 54-Hz P-wave transducers.

6 Results and Discussion

The Brazilian test was performed for 112 specimens in seven different orientations of lineation to the loading direction at 0°, 15°, 30°, 45°, 60°, 75° and 90°. To reproduce the peak strength data, two samples were tested for each orientation. However, the strain data have been acquired only for one specimen of each orientation. Classical equations for indirect tensile strength assume the rock to be homogenous, isotropic and brittle; therefore, they are not applicable to these anisotropic rocks. This paper uses the equation recommended by ISRM (1981) for indirect tensile strength only to represent the peak failure strength and not the tensile strength, as suggested by previous researchers (Barla and Innaurato 1973; Tavallali and Vervoort 2013).
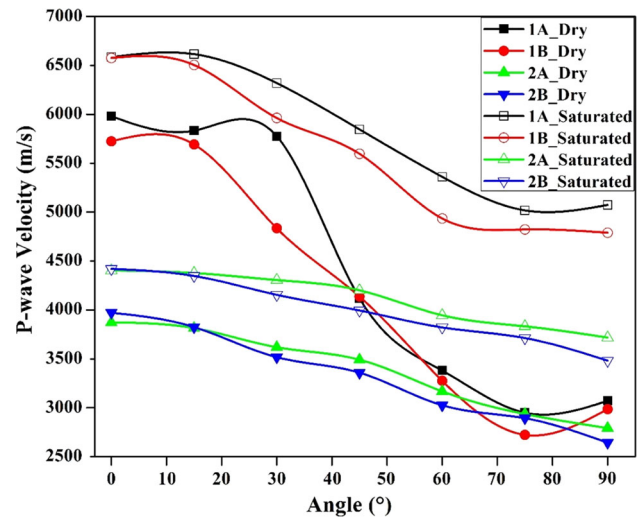

Fig. 10 Representation of P-wave velocity variation along different propagation direction with respect to the lineation, in both dry and saturated conditions of the rock samples

6.1 Dry Failure Strength

Both lineated mylonitic and crenulated schist show strength variation as a function of the β angle. Minimum strength is observed in between 20° and 60° of the β value
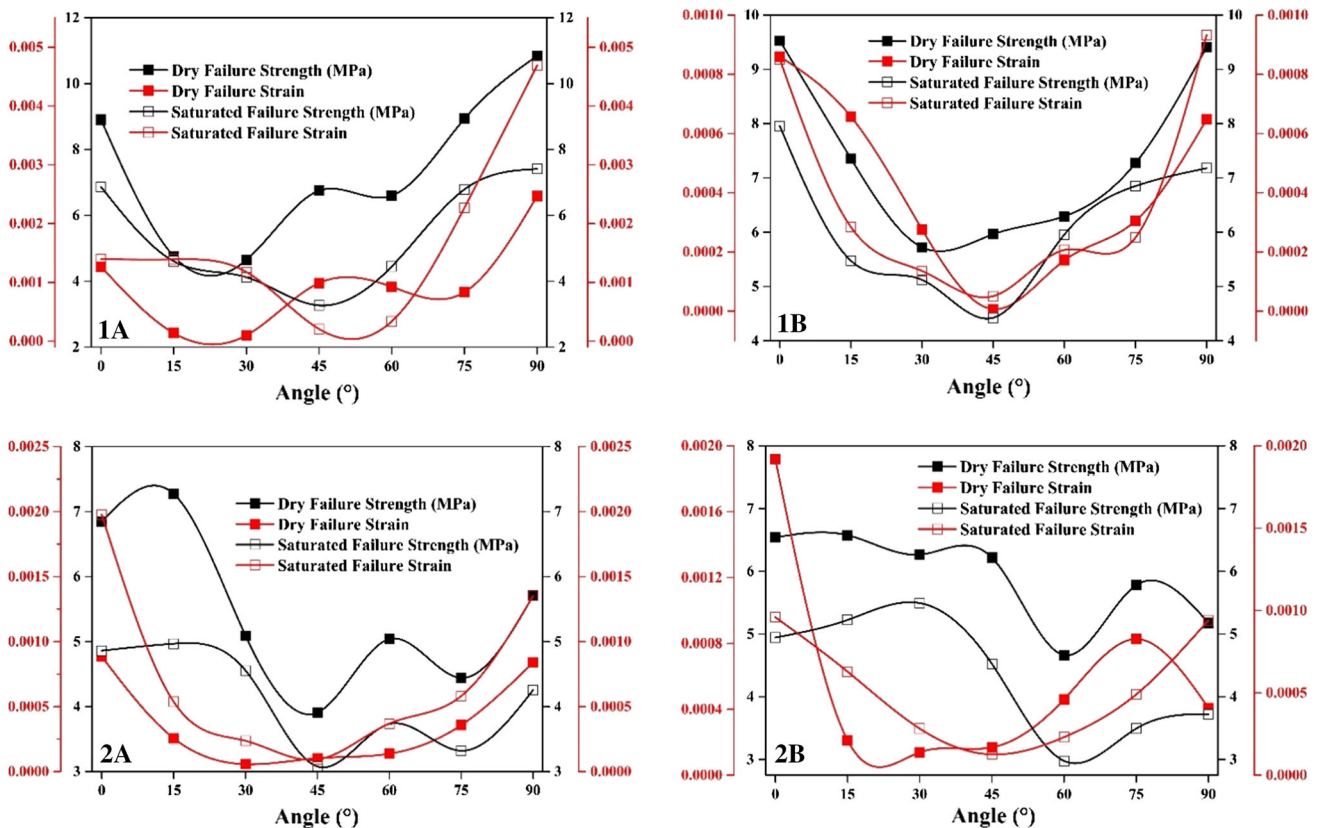

Fig. 9 Graphs representing failure strength and failure strain versus β angle in both dry and saturated conditions of specimen subtypes
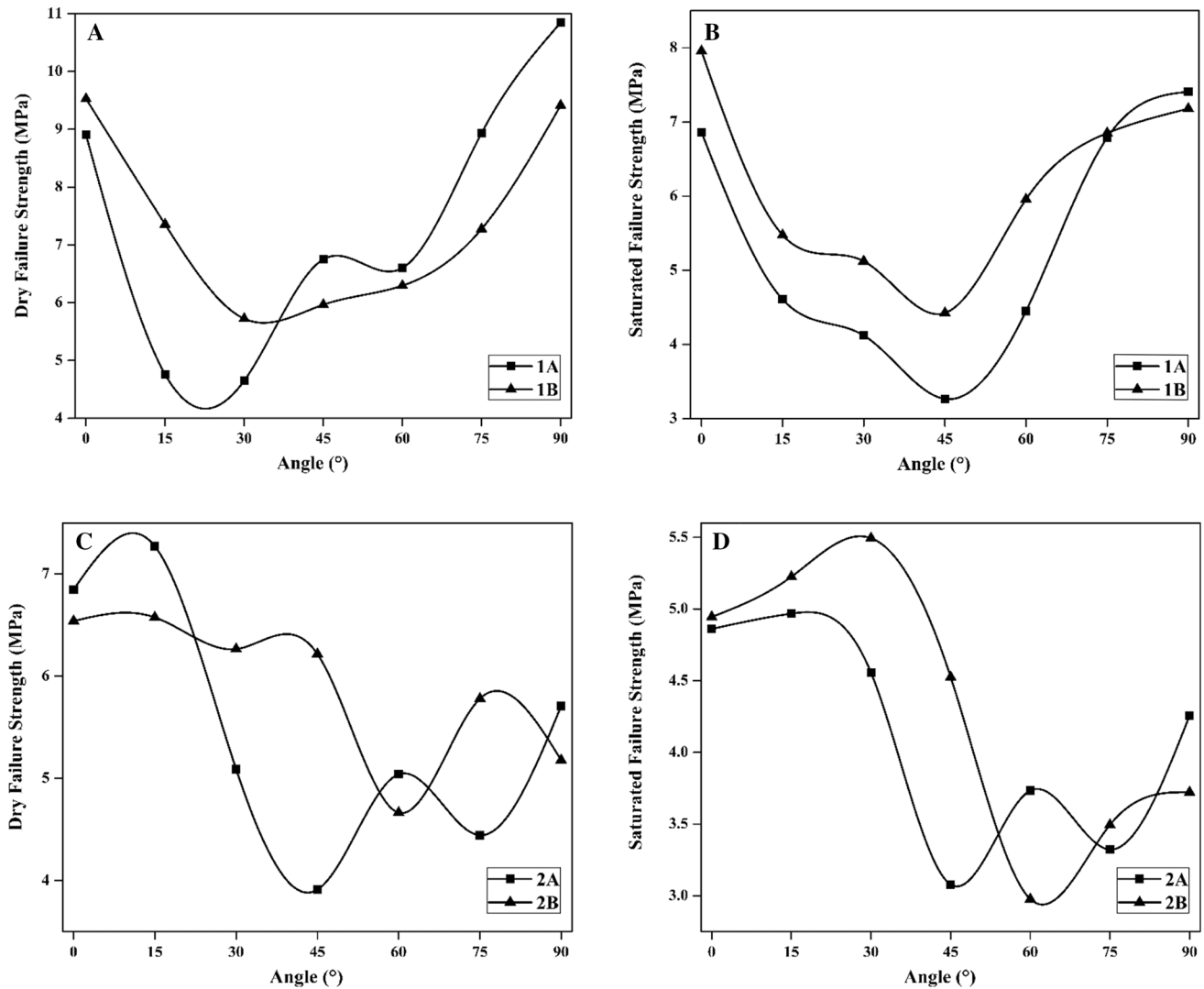
Fig. 11 Graph of failure strength versus orientation angle; **a** dry failure strength versus orientation angle of 1A and 1B; **b** saturated failure strength versus orientation angle of 1A and 1B; **c** dry failure strength versus orientation angle of 2A and 2B; **d** saturated failure strength versus orientation angle of 2A and 2B

(Fig. 9). Similar results have been reported by Barla and Innaurato (1973), Khanlari et al. (2015) and Tan et al. (2015). The strength minima for M-QMS vary from 20° to 30°, whereas for C-QMS the strength minima vary from 45° to 60°. The strength maxima for M-QMS are at 90°, while for C-QMS, the maxima are at 0°. Moreover, specimen 1A shows a greater anisotropic effect than 1B (Fig. 11a), which is parallel to the well-developed SSI (shows sigmoidal fabric in this plane). This effect may be attributed to the competence anisotropy around the mylonitic axis. Further study on axial anisotropy around mylonitic lineation for this type of rock would clarify the phenomena. Similarly, specimen 2A (the plane containing crenulation cleavage) shows a pronounced anisotropic effect in comparison with 2B (the plane that contains intersection cleavage) (Fig. 11c). The failure strain

anisotropy curve (failure strain versus β) for dry specimens follows approximately the same trend as of the strength anisotropy curve (peak strength versus β). The maximum failure strain is observed at 0° for M-QMS and at approx. 90° for C-QMS.

6.2 Effect of Water Saturation

It has been well established that water saturation has a significant effect on strength reduction in rock materials. A reduction in strength of even up to 90% in shale and mud rocks has been reported (Dyke and Dobereiner 1991; Hawkes and Mellor 1970; Vasarhelyi and Van 2006; Wong and Jong 2013). Wong et al. (2016) recently have reviewed the effects of water on the strength and stiffness degradation for sedimentary, igneous and metamorphic rocks.
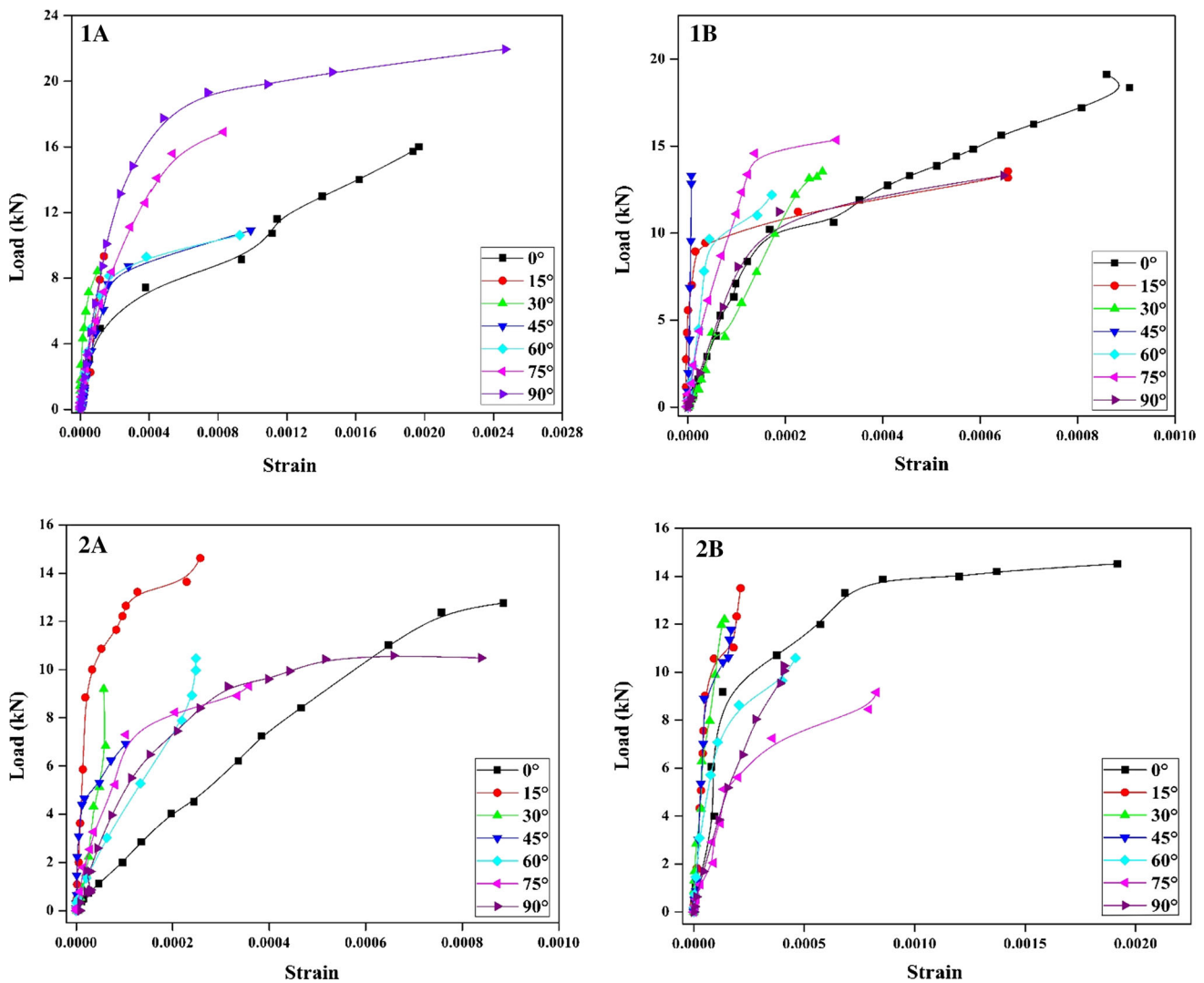
Fig. 12 Load versus strain graphs for dry specimens at all orientations

According to their study, due to water absorption effect, strength and modulus of sedimentary rocks are affected the most, while igneous and metamorphic rocks are affected less. Also, they concluded that though the water content is most significant in controlling rock strength and modulus, other internal and external factors such as porosity, density, fabric, strain rate and surface tension and dielectric constant of the saturating liquid play important roles. Gholami and Rasouli (2014), Van Eeckhout and Peng (1975) and White and Mazurkiewicz (1989) have represented the significant effect of water content on bedding or foliation-induced transverse anisotropy in rock. Although there have been extensive studies on the weakening effect of water, there probably have been no such previous observations of the water saturation effect on the strength anisotropic trend. Remarkable changes due to the effect of water in strength anisotropy have been noticed for M-QMS (Fig. 9). In addition to the decrease in the strength at each orientation,

the specimens show a shift in the strength minima towards a higher β angle. Although strength reduction is obvious at each orientation, there is no shift in the strength minima for C-QMS. A lower percentage of mica (16.4%) in C-QMS in comparison with M-QMS (37%) could be the possible explanation for such behaviour. Obreimoff and Kapitza (1930) have experimented on crack growth in cleaved mica with respect to different environments like dry or moist condition. The experiment resulted in rapid crack growth in moist air case than in vacuum due to low fracture surface energy in moist environment condition. Israelachvili et al. (1988) have also demonstrated the inverse relation of shear strength to the number of water layers present between mineral grains. Morrow et al. (2000) conducted an experiment on the effect of absorbed water on the frictional strength of different types of fault gauge materials and reported a significant reduction in the shear strength in micaceous minerals as a result of water absorption. After
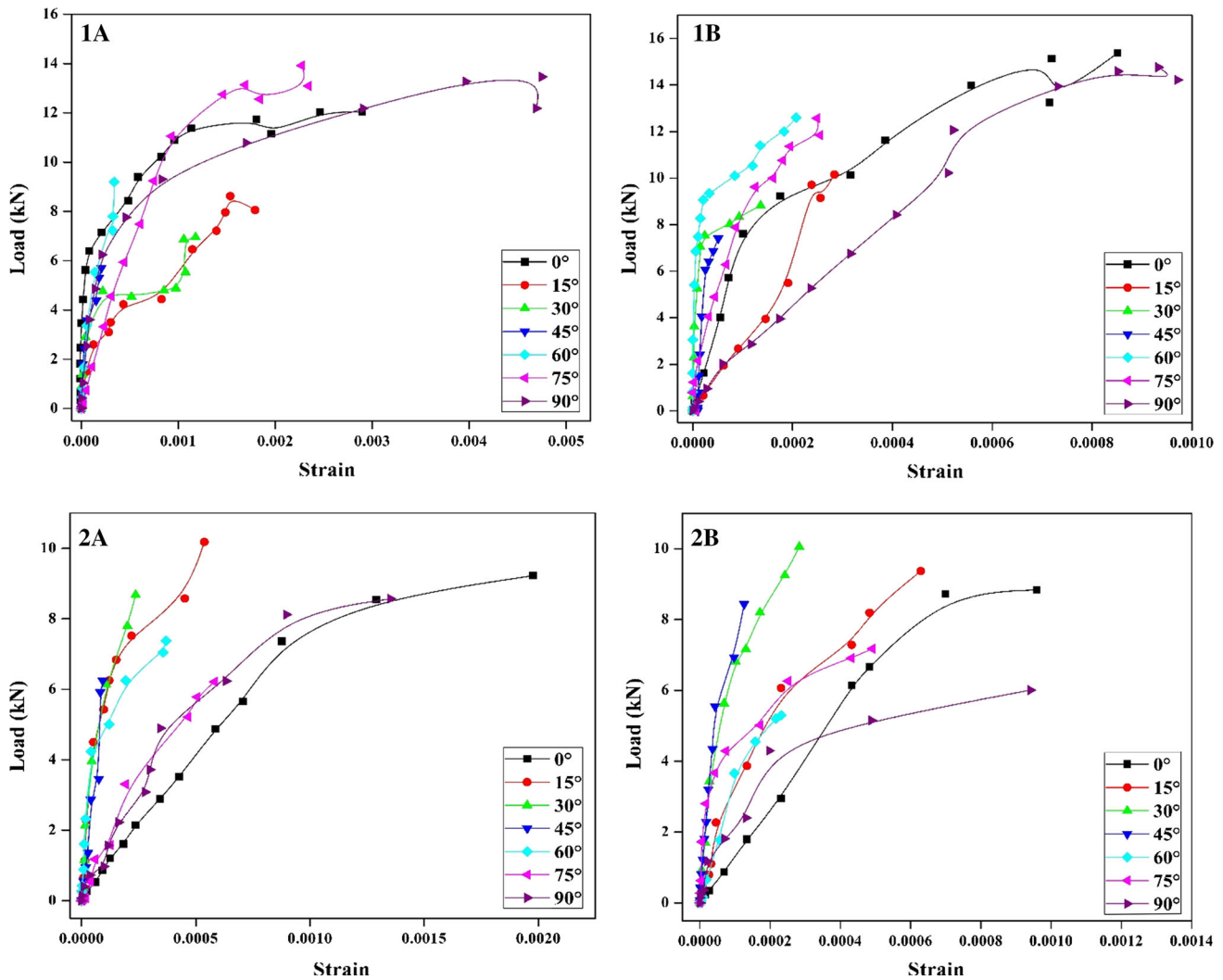
Fig. 13 Load versus strain graphs for saturated specimens at all orientations

saturation, they found around 20% reduction in shear strength in case of muscovite, while for quartz and feldspar, the effect was quite negligible (close to 0%). They explained that the charged surfaces of sheet-structure minerals absorb water more readily which effectively reduces the frictional resistance between particles. So, the shear strength reduction due to water would affect the micaceous layer at a greater level in comparison with the quartzo-feldspathic layer. The detailed structure of molecular water on mica surface has been published by Park and Sposito (2002). Specimen 1A has higher strength than 1B under saturated conditions (Fig. 11b), but no relation could be established between the saturated strength of 2A and 2B (Fig. 11d). It is clear from Fig. 9 that the effect of water on failure strain is prominent at 90° for M-QMS and at 0° for C-QMS.

It can be well inferred from the graph that the failure strength reduction percentage at each orientation is a result of water saturation for all specimen subtypes (Fig. 8). All

specimens show minimum strength reduction near 30° and an increasing trend thereafter, except for 2B, which has a minimum strength reduction at about 65° to the loading direction.

6.3 Strain Behaviour Along Lineation

The relationship between load and strain along lineation for the tested disc specimens in a dry condition is presented graphically in Figs. 12 and 13. The load versus strain graphs demonstrates a similar pattern for loading in a saturated condition. The maximum strain for 1A is 0.00026 at 45° in a dry condition, while it has been increased to 0.0048 at the same orientation in a saturated condition. For 1B, the maximum strain is 0.0009 (for a dry sample at 0°), which is almost unchanged in the saturated condition. The strain for all orientations for 1B is nearly unaffected in saturation. For 2A, maximum strain is 0.0009 in dry and 0.0020 in saturation at 0°. 2B displays a higher strain of
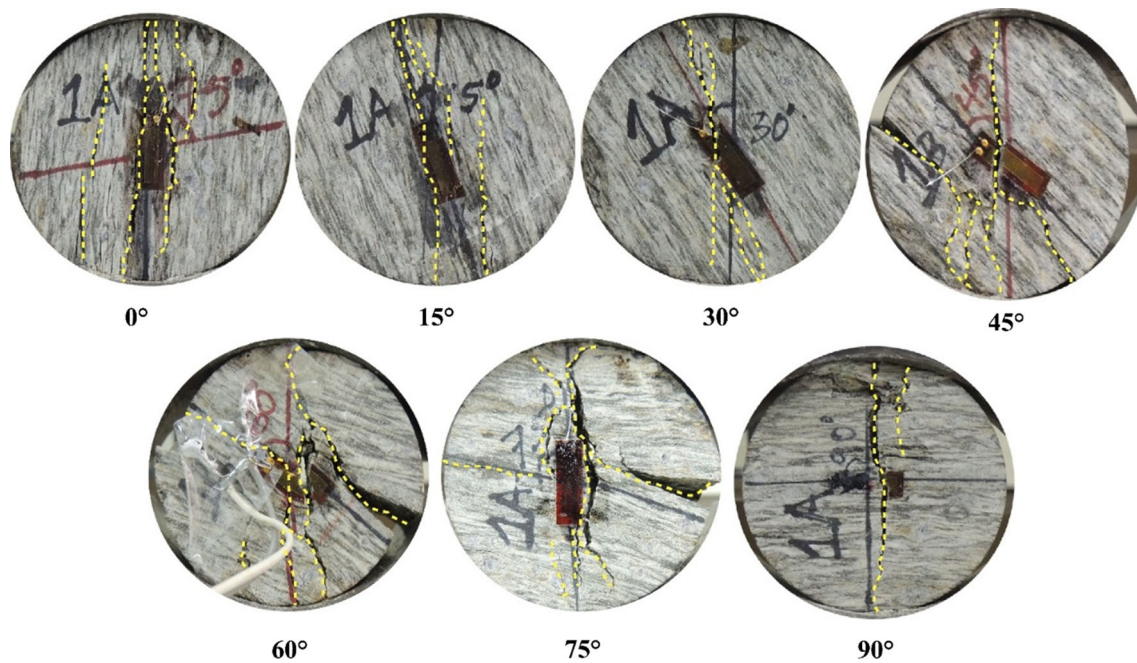
Fig. 14 Fracture patterns in the disc specimens of M-QMS showing the dependence of the fracture on the orientation of the lineation to the direction of loading
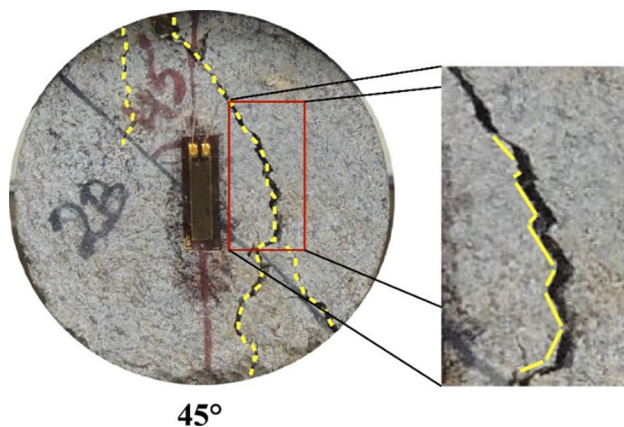

Fig. 15 Non-central fracture showing shear failure along the direction of lineation and tension detachment through the matrix

0.0020 at 0° in a dry condition and 0.0010 in saturation. In all graphs for the dry condition, specimens orienting at $\beta = 0°$ and 90° undergo more plastic deformation than other orientations. Moreover, a comparison of the dry load versus strain graph with the saturated load versus strain graph reveals the more ductile behaviour of specimens in saturated conditions.

6.4 P-Wave Velocity Anisotropy

The P-wave velocity has been determined in both dry and saturated conditions for both the rock types at different directions and varies from 0° to 90° with respect to the lineation. The P-wave velocity varies as a function of its propagation direction with respect to the lineation direction and shows a similar trend for all rock types and subtypes (1A, 1B, 2A and 2B). It shows maximum velocity along lineation and minimum across the lineation. Velocity variations for all subtypes are presented graphically in Fig. 10. Samples from M-QMS possess a higher anisotropy than the samples of C-QMS, which show a flattened curve (2A and 2B curves in Fig. 10). However, saturated samples show a higher velocity for all orientations and all rock types with a similar trend compared to dry specimens. It is observed that there is no similarity between strength anisotropy and anisotropy in the P-wave velocity.

6.5 Fracture Pattern

To demonstrate the fracture pattern in response to the inclination angle and strength, the patterns are described with respect to the orientation. It is observed that the fracture behaves differently for M-QMS and C-QMS. However, the fractures behave similarly for subtypes, for example, 1A and 1B for M-QMS. The fracture patterns in M-QMS follow the classifications of Tavallali and Vervoort (2010b). Three types of fractures are observed in this type of rock:

1. Layer activation: in which the fracture is parallel to the direction of lineation, with or without branches.
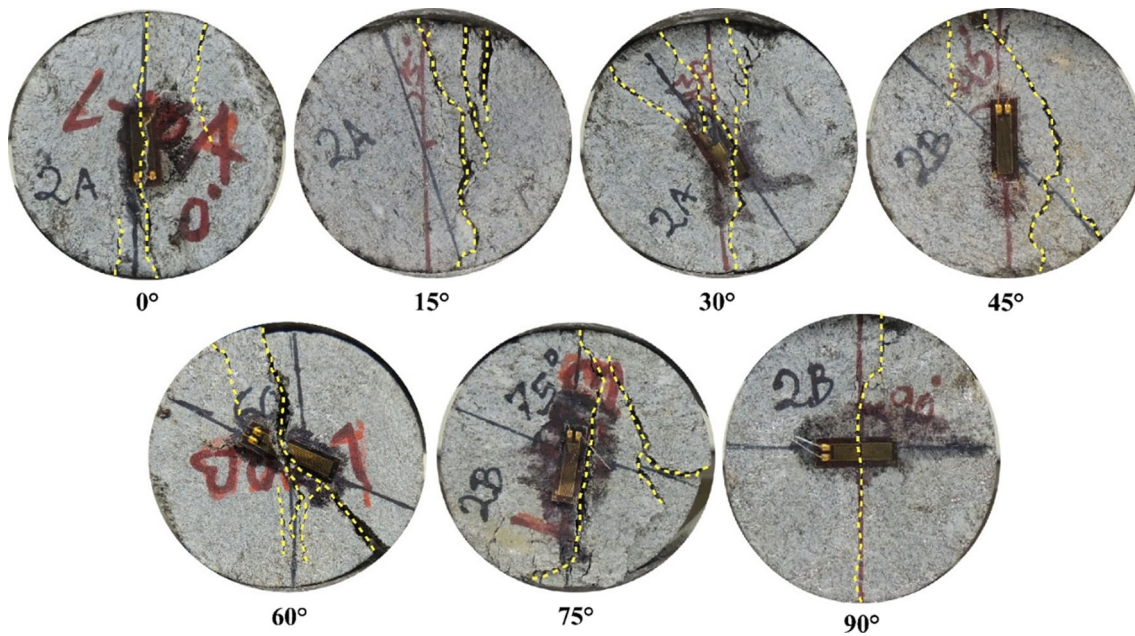
Fig. 16 Fracture patterns in the disc specimens of C-QMS, showing the dependence of the fracture on the orientation of the lineation to the loading direction

2. Central fracture: in which the fractures are parallel to the loading direction and are located in the area between 3 mm on either side of the loading line.
3. Non-central fractures: in which the fractures are outside the central region (the area between 3 mm on either side of the loading line) of the specimen.

The consideration of central region here is neither specified according to any established standard nor has any scientific justification. The consideration of central region in the area between 3 mm on either side of the loading line is rather arbitrary. Specimens from the M-QMS block show central fractures at β angle 0° and 90°. All other orientations show layer activation and non-central fractures. Non-central fractures in the specimen at 0° are believed to form after tensile failure along the loading line. Layer activation imposes its effect from 15° onwards up to 75°, but the process is dominant in between β angle of 45° and 60°. Layer activation in the specimens leads to shear fractures. Tensile failure is observed at the 0° and the 90° β angle case, whereas other orientations show the shear effect along the failure line. There is a continuous decrease in tensile component and a continuous increase in the shear component from 0° up to 60°; the effects again reverse from 60° to 90°. All the fracture patterns for M-QMS are illustrated in Fig. 14. The specimen with 90° orientation shows a crushing effect at the upper loading contact. In this small zone, the rock drops its stiffness and the surface flattens, forming loading contact of up to 50°. Debecker and Vervoort (2009) have also observed similar behaviour

in slate, which shows crushing and chipping of the rock at both the loading contacts.

Fracture patterns in the specimen of C-QMS correspond to the patterns for M-QMS specimens, but this rock type does not strictly hold the classification of Tavallali and Vervoort (2010b). The layer activation for this rock type is not pure; rather, it produces small step-like patterns in which it undergoes consecutive and frequent shear failure along the direction of lineation and tensional detachment through the matrix (Fig. 15). Specimens orienting at 0° and 90° show central and tensile fractures, whereas all other orientations fail in a mixed-mode condition, showing both the shear and the tension component. Specimens of C-QMS show a similar dependence of fracture on the inclination angle from 15° to 45°; this is unlike M-QMS, which shows an increasing shear behaviour. The difference in behaviour between these two rock types can be attributed to the difference in the stiffness of the lineation material and the matrix. Lineation frequency (lineation counts per cm) and its thickness may contribute to the process. Fracture patterns for C-QMS specimens are illustrated in Fig. 16. The yellow dotted lines in Figs. 14, 15 and 16 have been used to trace the fractures in deformed samples. It is again observed that fractures in case of saturated specimens are more mobilised along lineation (layer activation) than dry specimens. This layer activation is prominent in between the range of 15°–60° in the case of M-QMS (Fig. 17) and 15°–45° in the case of C-QMS (Fig. 18).
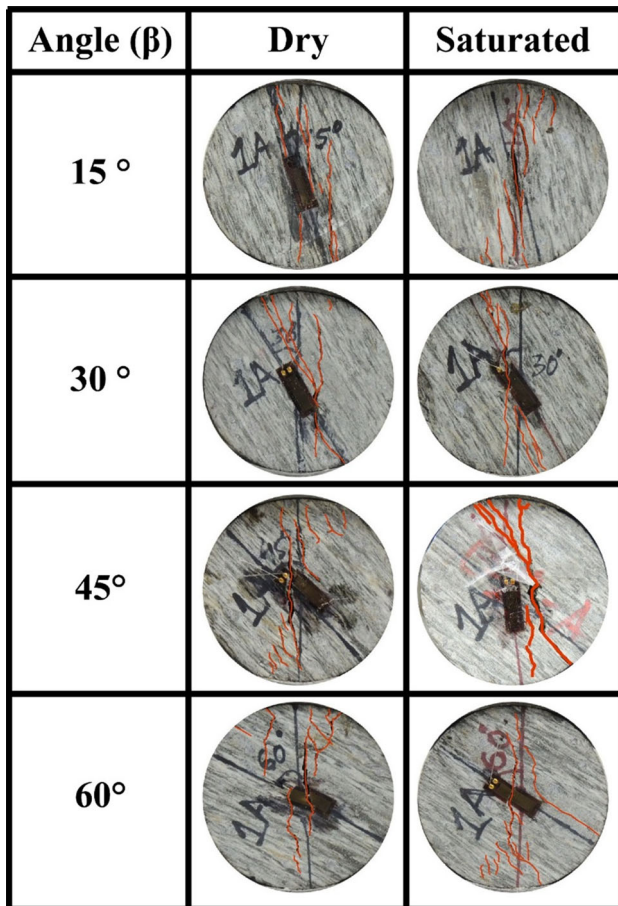
Fig. 17 Comparison of fracture patterns between dry and saturated specimens of M-QMS (block-1) at different orientations, showing prominent layer activation in case of saturated specimens. The *red line* on the tested specimen indicates the fracture pattern (colour figure online)

Fig. 18 Comparison of fracture patterns between dry and saturated specimens of C-QMS (block-2) at different orientations, showing prominent layer activation in case of saturated specimens. The *red line* on the specimen indicates the fracture pattern (colour figure online)

7 Conclusion

Literature survey on the anisotropic behaviour of rock materials provides comprehensive knowledge of transversely isotropic rocks that bear planner anisotropies for rock types such as sandstone, slate, shale, mud rocks, schists and gneiss. This experimental study on anisotropy considers lineation of mylonitic and crenulated schist as the subject. A systematic study of the effect of lineation on the strength, strain and P-wave velocity anisotropy shows that there is a considerable level of relation between the parameters and direction of lineation. The effect of water saturation is a new aspect in this study that was largely ignored in the previous literature.

The strength maxima for M-QMS are at 90° β, but the maxima are at 0° for C-QMS. The strength minima lie between 20° and 30° for M-QMS, while for C-QMS the strength minima lie between 45° and 60°. The mylonitic rock also possesses strength anisotropy in a plane perpendicular to the direction 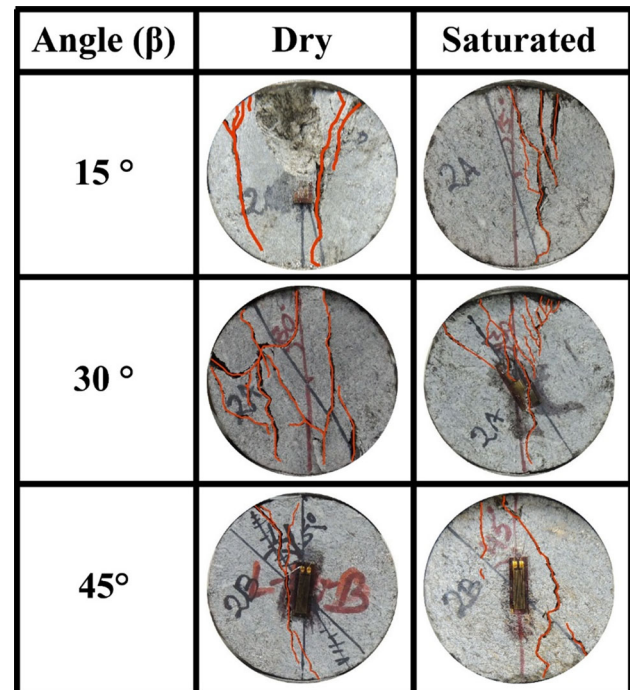of lineation. Strain along lineation also varies with respect to β, and strain anisotropy also shows a trend similar to strength anisotropy. Water saturation has a prominent effect on strength and its variation in response to a change in β. The strength of rocks is reduced drastically, and the effect is more pronounced when β is approx. 30°. There is a shift in the strength minima towards a higher β angle, and the shift amount may correspond to the percentage of mica in the rock. The rock, when saturated, is more plastic along lineation. The P-wave continuously decreases the velocity trend with an increase in the β angle.

Fractures in the specimens occur as central, non-central and lineation activation. Specimens with lineation that is parallel and perpendicular to the loading direction break in pure tension, whereas other orientations break in a mixed mode (both in tension and in shear). In M-QMS, there is a greater dependency of the fracture pattern in the direction of lineation when compared to C-QMS. Fracture through the layer activation is prominent in saturated specimens than the dry specimens, especially in the range of 15°–60° in the case of M-QMS and 15°–45° for C-QMS. The shear behaviour of fractures continuously increases up to 60° and then decreases to pure tensile at 90°.

allowing to conduct all geotechnical experiments and other necessary supports.

References

Amadei B (1996) Importance of anisotropy when estimating and measuring in situ stresses in rock. Int J Rock Mech Min Sci Geomech Abstr 33:293–325. doi:10.1016/0148-9062(95)00062-3

Amadei B, Savage WZ, Swolfs HS (1987) Gravitational stresses in anisotropic rock masses. Int J Rock Mech Min Sci Geomech Abstr 24:5–14. doi:10.1016/0148-9062(92)93657-6

ASTM D3967-08 (2008) Standard test method for splitting tensile strength of intact rock core specimens 1. ASTM Int., West Conshohocken, PA, pp 20–23. doi:10.1520/D3967-08.2

Barla G, Innaurato N (1973) Indirect tensile testing of anisotropic rocks. Rock Mech Rock Eng 5:215–230. doi:10.1007/BF01301795

Berenbaom R, Brodie I (1959) The tensile strength of coal. J Inst Fuel 32:320–327

Bhargava ON (1972) A note on the Rampur window, District Mahasu, H. P. Geol Soc India 13:277–280. doi:10.1136/hrt.10.2.99

Cai M, Kaiser PK (2004) Numerical simulation of the Brazilian test and the tensile strength of anisotropic rocks and rocks with pre-existing cracks. Int J Rock Mech Min Sci 41:1–6. doi:10.1016/j.ijrmms.2004.03.086

Casagrande A, Carillo N (1944) Shear failure of anisotropic materials. Boston Soc Civil Eng 31:74–87

Chen CS, Hsu SC (2001) Measurement of indirect tensile strength of anisotropic rocks by the ring test. Rock Mech Rock Eng 34:293–321. doi:10.1007/s006030170003

Chen C, Pan E, Amadei B (1998) Determination of deformability and tensile strength of anisotropic rock using Brazilian tests. Int J Rock Mech Min Sci Geomech Abstr 35:43–61. doi:10.1016/S0148-9062(97)00329-X

Claesson J, Bohloli B (2002) Brazilian test: stress field and tensile strength of anisotropic rocks using an analytical solution. Int J Rock Mech Min Sci 39:991–1004. doi:10.1016/S1365-1609(02)00099-0

Davis GH, Reynolds SJ, Kluth C (2012) Structural geology of rocks and regions. Wiley, Hoboken

Debecker B, Vervoort A (2009) Experimental observation of fracture patterns in layered slate. Int J Fract 159:51–62. doi:10.1007/s10704-009-9382-z

Donath F (1961) Experimental study of shear failure in anisotropic rocks. Geol Soc Am Bull 72:985–990

Donath FA, Cohen CI (1960) Anisotropy and failure in rocks. Bull Geol Soc Am 71:1851

Dyke CG, Dobereiner L (1991) Evaluating the strength and deformability of sandstones. Q J Eng Geol Hydrogeol 24:123–134. doi:10.1144/GSL.QJEG.1991.024.01.13

Fairhurst C (1964) On the validity of the "Brazilian" test for brittle materials. Int J Rock Mech Min Sci Geomech Abstr 1:535–546. doi:10.1016/0148-9062(64)90060-9

Fereidooni D, Khanlari GR, Heidari M, Sepahigero AA, Kolahi-Azar AP (2015) Assessment of inherent anisotropy and confining pressure influences on mechanical behavior of anisotropic foliated rocks under triaxial compression. Rock Mech Rock Eng 49:2155–2163. doi:10.1007/s00603-015-0814-y

Gholami R, Rasouli V (2014) Mechanical and elastic properties of transversely isotropic slate. Rock Mech Rock Eng 47:1763–1773. doi:10.1007/s00603-013-0488-2

Gong QM, Zhao J, Jiao YY (2005) Numerical modeling of the effects of joint orientation on rock fragmentation by TBM cutters. Tunn Undergr Space Technol 20:183–191. doi:10.1016/j.tust.2004.08.006

Gray DR, Durney DW (1979) Crenulation cleavage differentiation: implications of solution-deposition processes. J Struct Geol 1:73–80. doi:10.1016/0191-8141(79)90023-3

Hawkes I, Mellor M (1970) Uniaxial testing in rock mechanics laboratories. Eng Geol 4:177–285

Hobbs DW (1964) The tensile strength of rocks. Int J Rock Mech Min Sci Geomech Abstr 1:335–396. doi:10.1016/0009-2509(68)89051-7

Hobbs DW (1965) An assessment of a technique for determining the tensile strength of rock. Br J Appl Phys 16:259–268

Hobbs BE, Means WD, Williams PF (1976) An outline of structural geology. Wiley, New York

Hoek E (1964) Fracture of anisotropic rock. J S Afr Inst Min Metall 64:501–518

Hudson JA (1969) Tensile strength and the ring test. Int J Rock Mech Min Sci Geomech Abstr 6:91–97. doi:10.1016/0148-9062(69)90029-1

Israelachvili JN, McGuiggan PM, Homola AM (1988) Dynamic properties of molecularly thin liquid films. Science 240:189–191

ISRM (1981) The ISRM suggested methods for rock characterization, testing and monitoring. Pergamon Press, Oxford

Jaeger JC (1960) Shear failure of anistropic rocks. Geol Mag 97:65–72

Khanlari G, Rafiei B, Abdilor Y (2015) An experimental investigation of the Brazilian tensile strength and failure patterns of laminated sandstones. Rock Mech Rock Eng 48:843–852. doi:10.1007/s00603-014-0576-y

Kim KY, Zhuang L, Yang H, Kim H, Min KB (2016) Strength anisotropy of Berea sandstone: results of X-ray computed tomography, compression tests, and discrete modeling. Rock Mech Rock Eng 49:1201–1210. doi:10.1007/s00603-015-0820-0

Kundu J, Mahanta B, Tripathy A, Sarkar K, Singh TN (2016a) Stability evaluation of jointed rock slope with curved face. In: INDOROCK 2016. Mumbai, India, pp 971–978

Kundu J, Sarkar K, Singh AK (2016b) Integrating structural and numerical solutions for road cut slope stability analysis-a case study, India. In: Proceedings of the 2nd international conference on rock dynamics and applications, pp 457–462

Li D, Wong LNY (2013) The Brazilian disc test for rock mechanics applications: review and new insights. Rock Mech Rock Eng 46:269–287. doi:10.1007/s00603-012-0257-7

Lin C, He J, Li X, Wan X, Zheng B (2016) An experimental investigation into the effects of the anisotropy of shale on hydraulic fracture propagation. Rock Mech Rock Eng 50:543–554. doi:10.1007/s00603-016-1136-4

Mahanta B, Singh HO, Singh PK, Kainthola A, Singh TN (2016a) Stability analysis of potential failure zones along NH-305, India. Nat Hazards 83:1341–1357. doi:10.1007/s11069-016-2396-8

Mahanta B, Singh TN, Ranjith PG (2016b) Influence of thermal treatment on mode I fracture toughness of certain Indian rocks. Eng Geol 210:103–114. doi:10.1016/j.enggeo.2016.06.008

McLamore R, Gray KE (1967) The mechanical behavior of anisotropic fine-grained sedimentary roks. J Eng Ind 89:62–73

Mellor M, Hawkes I (1971) Measurement of tensile strength by diametral compression of discs and annuli. Eng Geol 5:173–225. doi:10.1016/0013-7952(71)90001-9

Mighani S, Sondergeld CH, Rai CS (2016) Observations of tensile fracturing of anisotropic rocks. Soc Pet Eng (Preprint)

Morrow C, Moore DE, Lockner DA (2000) The effect of mineral bond strength and adsorbed water on fault gouge frictional strength. Geophys Res Lett 27:815–818. doi:10.1029/1999GL008401

Mukhopadhaya DK, Ghosh TK, Bhadra BK, Srivastava DC (1997) Structural and metamorphic evolution of the rocks of the Jutogh Group, Chur half-klippe, Himachal Himalayas: a summary and

comparison with the Simla area. In: Proceedings of the Indian academy of sciences- earth and planetary sciences, pp 197–207

Nasseri MHB, Rao KS, Ramamurthy T (2003) Anisotropic strength and deformation behavior of Himalayan schists. Int J Rock Mech Min Sci 40:3–23. doi:10.1016/S1365-1609(02)00103-X

Nova R, Zaninetti A (1990) An investigation into the tensile behaviour of a schistose rock. Int J Rock Mech Min Sci Geomech Abstr 27:231–242. doi:10.1016/0148-9062(90)90526-8

Obreimoff JW, Kapitza P (1930) The splitting strength of mica. In Proceedings of the royal society of London A, pp 290–297. doi:10.1098/rsta.1979.0079

Ogunsanwo O (1986) Influence of angle of inclination of schistosity planes on the geotechnical properties of a schist saprolite. Eng Geol 23:137–143

Pan E, Amadei B, Savage WZ (1994) Gravitational stresses in long symmetric ridges and valleys in anisotropic rock. Int J Rock Mech Min Sci Geomech Abstr 31:293–312

Pan E, Amadei B, Savage WZ (1995) Gravitational and tectonic stresses in anisotropic rock with irregular topography. Int J Rock Mech Min Sci Geomech Abstr 32:201–214. doi:10.1016/0148-9062(94)00046-6

Pandey AK, Sachan HK, Virdi NS (2004) Exhumation history of a shear zone constrained by microstructural and fluid inclusion techniques: an example from the Satluj valley, NW Himalaya, Indian. J Asian Earth Sci 23:391–406. doi:10.1016/S1367-9120(03)00167-6

Park S-H, Sposito G (2002) Structure of water adsorbed on a mica surface. Phys Rev Lett 89:85501. doi:10.1103/PhysRevLett.89.085501

Passchier CW, Trouw RAJ (2005) Microtectonics. Springer, Berlin

Ramamurthy T, Arora VK (1994) Strength predictions for jointed rocks in confined and unconfined states. Int J Rock Mech Min Sci Geomech Abstr 31:9–22

Salamon MDG (1968) Elastic moduli of a stratified rock mass. Int J Rock Mech Min Sci 5:519–527. doi:10.1016/0148-9062(68)90039-9

Singh K (1979) Deformation history of the rocks around Sarahan Bushair, Himachal Pradesh. In: Saklani PS (ed) Structural geology of the Himalaya. Today and Tomorrow's Printers & Publishers, New Delhi, pp 163–182

Singh M, Samadhiya NK, Kumar A, Kumar V, Singh B (2015) A nonlinear criterion for triaxial strength of inherently anisotropic rocks. Rock Mech Rock Eng 48:1387–1405. doi:10.1007/s00603-015-0708-z

Stjern G, Agle A, Horsrud P (2003) Local rock mechanical knowledge improves drilling performance in fractured formations at the Heidrun field. J Pet Sci Eng 38:83–96. doi:10.1016/S0920-4105(03)00023-8

Talesnick ML, Lee MY, Haimson BC (1995) On the determination of elastic material parameters of transverse isotropic rocks from a single test specimen. Rock Mech Rock Eng 28:17–35. doi:10.1007/BF01024771

Tan X, Konietzky H, Frühwirt T, Dan DQ (2015) Brazilian tests on transversely isotropic rocks: laboratory testing and numerical simulations. Rock Mech Rock Eng 48:1341–1351. doi:10.1007/s00603-014-0629-2

Tavallali A (2010) Failure of layered Modave sandstone: Effect of layer orientation and material properties. PhD Thesis. Department of Civil Engineering, Katholieke Universiteit Leuven

Tavallali A, Vervoort A (2010a) Failure of layered sandstone under Brazilian test conditions: effect of micro-scale parameters on macro-scale behaviour. Rock Mech Rock Eng 43:641–653. doi:10.1007/s00603-010-0084-7

Tavallali A, Vervoort A (2010b) Acoustic emission monitoring of layered sandstone under Brazilian test conditions. In: Rock mechanics in civil and environmental engineering, pp 91–94

Tavallali A, Vervoort A (2013) Behaviour of layered sandstone under Brazilian test conditions: layer orientation and shape effects. J Rock Mech Geotech Eng 5:366–377. doi:10.1016/j.jrmge.2013.01.004

Van Eeckhout EM, Peng SS (1975) The effect of humidity on the compliances of coal mine shales. Int J Rock Mech Min Sci Geomech Abstr 12:335–340. doi:10.1016/0148-9062(75)90166-7

Vasarhelyi B, Van P (2006) Influence of water content on the strength of rock. Eng Geol 84:70–74. doi:10.1016/j.enggeo.2005.11.011

Vervoort A, Min KB, Konietzky H, Cho JW, Debecker B, Dinh QD, Frühwirt T, Tavallali A (2014) Failure of transversely isotropic rock under Brazilian test conditions. Int J Rock Mech Min Sci 70:343–352. doi:10.1016/j.ijrmms.2014.04.006

Wardle LJ, Gerrard CM (1972) The "equivalent" anisotropic properties of layered rock and soil masses. Rock Mech Rock Eng 4:155–175. doi:10.1007/BF01597000

White JM, Mazurkiewicz M (1989) Effect of moisture content on mechanical properties of Nemo coal, Moberly, Missouri USA. Min Sci Technol 9:181–185

Wong L, Jong M (2013) Water saturation effects on the Brazilian tensile strength of gypsum and assessment of cracking processes using high-speed video. Rock Mech Rock Eng 47:1103–1115

Wong LNY, Maruvanchery V, Liu G (2016) Water effects on rock strength and stiffness degradation. Acta Geotech 11:713–737. doi:10.1007/s11440-015-0407-7

Zhang XP, Wong LNY, Wang SJ, Han GY (2011) Engineering properties of quartz mica schist. Eng Geol 121:135–149. doi:10.1016/j.enggeo.2011.04.020

Zhang XP, Wu S, Afolagboye LO, Wang S, Han G (2015) Using the point load test to analyze the strength anisotropy of quartz mica schist along an exploration adit. Rock Mech Rock Eng 49:1967–1975. doi:10.1007/s00603-015-0792-0